Transport, magnetic, and magnetotransport properties of $Ba_{3-x}R_xTa_5O_{15}$ (R = rare earth)

Haruki Takei [1], Satomi Ito,[1] Kenta Iwamoto,[1] Yumiko Katayama [2], Kazunori Ueno,[2]
Hideki Kuwahara [3], and Takuro Katsufuji [1,4]

[1]*Department of Physics, Waseda University, Tokyo 169-8555, Japan*
[2]*Department of Basic Science, University of Tokyo, Meguro, Tokyo 153-8902, Japan*
[3]*Department of Physics, Sophia University, Tokyo 169-8555, Japan*
[4]*Kagami Memorial Research Institute for Materials Science and Technology, Waseda University, Tokyo 169-0051, Japan*

Barium tantalate with a tetragonal tungsten bronze structure, $Ba_3Ta_5O_{15}$, and compounds where Ba is partly substituted by various rare earths (R), $Ba_{3-x}R_xTa_5O_{15}$, were synthesized as single crystals, and their transport, magnetic, and magnetotransport properties were investigated. It was found that the compounds with Eu substitution show a relatively large negative magnetoresistance arising from the interaction between the conduction electrons in the Ta $5d$ orbital and the localized spins in the Eu $4f$ orbital.

I. INTRODUCTION

$Ba_3Nb_5O_{15}$ [1–12] is a compound with a tetragonal tungsten bronze structure and exhibits metallic behavior due to 0.2 electrons per Nb in the $4d$ orbitals. In this compound, the resistivity along the c axis is approximately one order of magnitude lower than that along the ab plane [8,11], and such anisotropy is attributed to the different configuration of Nb-O-Nb, which is arranged in a straight manner along the c axis but in a zigzag manner along the ab plane, as shown in Fig. 1. This compound becomes superconducting below 1.5 K [6]. With the substitution of Ba by Sr or Eu, $Ba_{3-x}Sr_xNb_5O_{15}$ and $Ba_{3-x}Eu_xNb_5O_{15}$ exhibit a metal-insulator transition at the x value of approximately 2, similarly to some other $4d$ oxides [13–16], although both Ba and Sr or Eu are divalent and the substitution does not change the nominal number of d electrons in Nb. Near the metal-insulator phase boundary, $Ba_{3-x}Eu_xNb_5O_{15}$ exhibits a large negative magnetoresistance of $\rho(0)/\rho(H) \sim 10^4$ [9,11], where $\rho(H)$ is the resistivity at the magnetic field of H. Such a peculiar behavior is attributed to the coupling between the itinerant electrons in the $4d$ orbitals of Nb and the localized spins in the $4f$ orbitals of Eu, similarly to several oxides or chalcogenides including Eu^{2+} ions [17–24]. As a possible mechanism of the further enhancement of negative magnetoresistance, it is proposed that magnetic polarons are formed in $Ba_{3-x}Eu_xNb_5O_{15}$ [11], similarly to Eu oxides or chalcogenides [17–20]. According to a photoemission spectroscopy of this series of compounds [12], Eu $4f$ levels exist ~ 2 eV below the Fermi level, and a core level of Nb is well screened for $x = 2$ but is not for $x = 3$, consistent with the metal-insulator transition at $x \sim 2.2$. On the other hand, with the substitution of Ba by trivalent rare earths, $Ba_{3-x}R_xNb_5O_{15}$ remains metallic up to $x = 1$ with a decrease in the absolute values of the Hall coefficient and Drude weight in the optical conductivity spectrum [11].

$Ba_3Ta_5O_{15}$ [26–29] is known to have the same crystal structure as $Ba_3Nb_5O_{15}$. Although different physical properties arising from the $5d$ orbitals of Ta, which are more extended in space than the $4d$ orbitals of Nb, are expected, only the crystal structure, but not the physical properties, has been reported for the Ta compound. Note that only a few Ta oxides have metallic properties caused by $5d$ electrons, but W [30–32], Re [33,34], Os [35–37], and Ir [38–42] oxides with metallic properties are well known, some of which exhibit intriguing physical properties arising from the strong spin-orbit coupling of $5d$ electrons. Furthermore, by substituting Ba with rare earths in $Ba_3Ta_5O_{15}$, we can study how the coupling between the conduction electrons in the Ta $5d$ orbitals and the localized moments in the rare-earth $4f$ orbitals affects the physical properties, as in the case of the Nb compounds exhibiting a large magnetoresistance.

In this study, we grew single crystals of $Ba_3Ta_5O_{15}$ and those with the substitution of Ba by a trivalent or divalent rare earth, $Ba_{3-x}R_xNb_5O_{15}$ (R = La, Ce, Pr, Nd, Sm, Eu, Gd, Tb, Dy, Ho, Er, and Tm), and investigated their transport, magnetic, and optical properties. In particular, we focus on the magnetoresistance arising from the coupling between the $5d$ conduction electrons of Ta and the $4f$ moments of the rare earth.

II. EXPERIMENT

We grew single crystals of $Ba_{3-x}R_xTa_5O_{15}$ using the floating-zone technique [43–45]. The starting materials were Ta, Ta_2O_5, $Ba_5Ta_4O_{15}$, and rare-earth oxides (R_2O_3 except for CeO_2 for Ce and Tb_4O_7 for Tb). $Ba_5Ta_4O_{15}$ was prepared by calcining stoichiometric amounts of $BaCO_3$ and Ta_2O_5 at 1200 °C for 20 h in air. To prepare a polycrystalline rod, stoichiometric amounts of the starting materials were mixed, pressed into a rod, and sintered at 1350 °C for 30 h in a flow of 7% H_2/Ar gas. Subsequently, the sintered rod was melt-grown using a floating-zone furnace in a flow of 7% H_2/Ar gas.

The quality and lattice constants of the grown crystals were determined by x-ray powder diffraction measurements. It was found that $Ba_{3-x}R_xTa_5O_{15}$ with $x > 1$ cannot be grown except

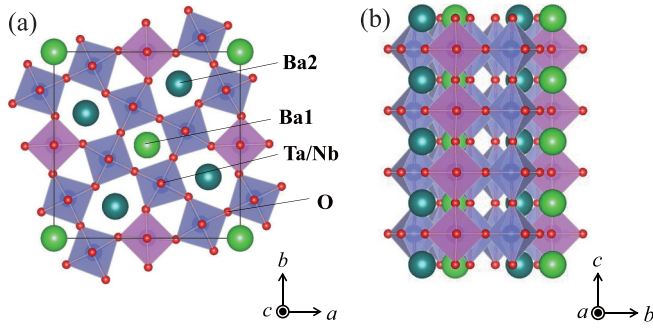FIG. 1. Crystal structures of $Ba_3Ta_5O_{15}$ and $Ba_3Nb_5O_{15}$ viewed from the (a) c and (b) a axes drawn using VESTA [25].

for $R =$ Eu. The orientation of the grown single crystals was determined by the Laue method. The valence of Ta in the grown crystals was determined by thermogravimetric analysis (TGA). In this measurement, except for $R =$ Eu, only the valence of Ta changes from 4+ to 5+ upon the oxidization of the sample and, thus, it is highly sensitive and reliable for the estimate of the Ta valence. It is to be noted that for $R =$ Eu, the valence of Eu also changes from 2+ to 3+ upon oxidization, and this is taken into account when the Ta valence of the Eu-doped samples is estimated.

Electrical resistivity, magnetoresistance, and Hall resistivity were measured using a Physical Properties Measurement System (PPMS) with gold paste cured at room temperature as electrodes. For the magnetoresistance and Hall resistivity measurements, a magnetic field was applied in the range of -7 and 7 T perpendicular to the current direction. Magnetic susceptibility was measured using a SQUID magnetometer. Polarized optical reflectivity was measured at room temperature on the polished ac plane of the grown crystals using a grating spectrometer from 0.7 to 5 eV and an FTIR spectrometer from 0.1 to 0.8 eV.

III. RESULTS

First, the data of the parent compound $Ba_3Ta_5O_{15}$ are shown in comparison with those of $Ba_3Nb_5O_{15}$. Figure 2(a) shows the temperature (T) dependence of resistivity along the c (ρ_c) and a (ρ_a) axes for $Ba_3Ta_5O_{15}$ (solid lines) and $Ba_3Nb_5O_{15}$ (dashed lines) reported in Ref. [8]. As can be seen, ρ_c is one order of magnitude lower than ρ_a for $Ba_3Ta_5O_{15}$, similarly to $Ba_3Nb_5O_{15}$. This indicates a higher electrical conductivity along the direction of straight Ta-O chains along the c axis (Fig. 1). However, the upturn of ρ_a at low T observed for $Ba_3Nb_5O_{15}$ is not observed for $Ba_3Ta_5O_{15}$, which exhibits a positive $d\rho/dT$ for both ρ_c and ρ_a at all temperatures. This indicates that the electronic conduction is less anisotropic for the present $Ba_3Ta_5O_{15}$ than for $Ba_3Nb_5O_{15}$.

Reflectivity spectra with the polarization along the c [$R_c(\omega)$] and a [$R_a(\omega)$] axes at room temperature are shown in Figs. 3(a) and 3(b), respectively, for $Ba_3Ta_5O_{15}$ (solid lines) and $Ba_3Nb_5O_{15}$ (dashed lines) [8]. The reflectivity of $Ba_3Ta_5O_{15}$ decreases gradually with increasing $\hbar\omega$ and exhibits a dip (a plasma edge), a typical spectrum for a metallic state, both for $R_c(\omega)$ and $R_a(\omega)$. R_c is higher than R_a below the plasma edge and the position of the plasma edge $\hbar\omega_p$
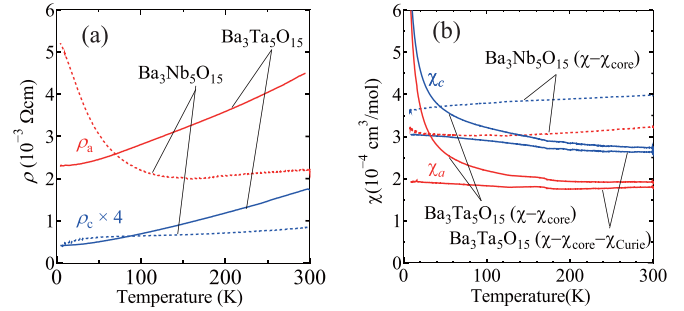

FIG. 2. (a) Temperature dependence of resistivity of $Ba_3Ta_5O_{15}$ (solid lines) and $Ba_3Nb_5O_{15}$ (dashed lines) along the c (blue) and a (red) axes. The data along the c axis are multiplied by four for both compounds. (b) Temperature dependence of magnetic susceptibility of $Ba_3Ta_5O_{15}$ (solid lines) and $Ba_3Nb_5O_{15}$ (dashed lines) along the c (χ_c, blue) and a (χ_a, red) axes. Larmor diamagnetism arising from the core electrons at each atom is subtracted from each of the data. For the data of $Ba_3Ta_5O_{15}$, those from which the Curie component $C/(T + \theta)$ has been subtracted are also plotted.

(plasma frequency) for R_c ($\sim$1.1 eV) is higher in energy than that for R_a ($\sim$0.8 eV). These characteristics are the same as those for $Ba_3Nb_5O_{15}$. Regarding the comparison between the two compounds, the reflectivity of $Ba_3Ta_5O_{15}$ below $\hbar\omega_p$ is lower than that of $Ba_3Nb_5O_{15}$, and the $\hbar\omega_p$ of $Ba_3Ta_5O_{15}$ is smaller than that of $Ba_3Nb_5O_{15}$, both for R_c and R_a.

Optical conductivity spectra along the c [$\sigma_c(\omega)$] and a [$\sigma_a(\omega)$] axes derived from the reflectivity spectra by the Kramers-Kronig transformation are shown in Figs. 3(c) and 3(d), respectively. The spectral weight below 1 eV, corresponding to the Drude weight, for $\sigma_c(\omega)$ is larger than that
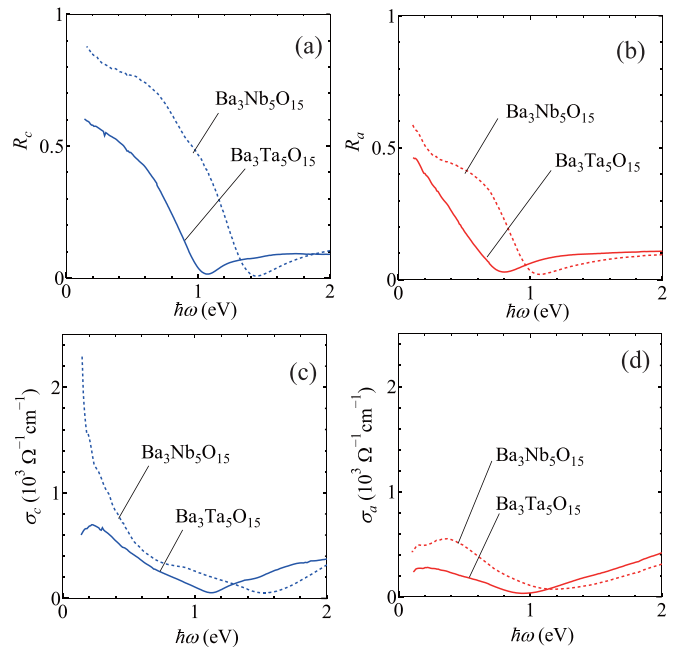

FIG. 3. (a), (b) Reflectivity spectra with the polarization along the (a) c and (b) a axes, and (c), (d) optical conductivity spectra along the (c) c and (d) a axes for $Ba_3Ta_5O_{15}$ (solid lines) and $Ba_3Nb_5O_{15}$ (dashed lines).
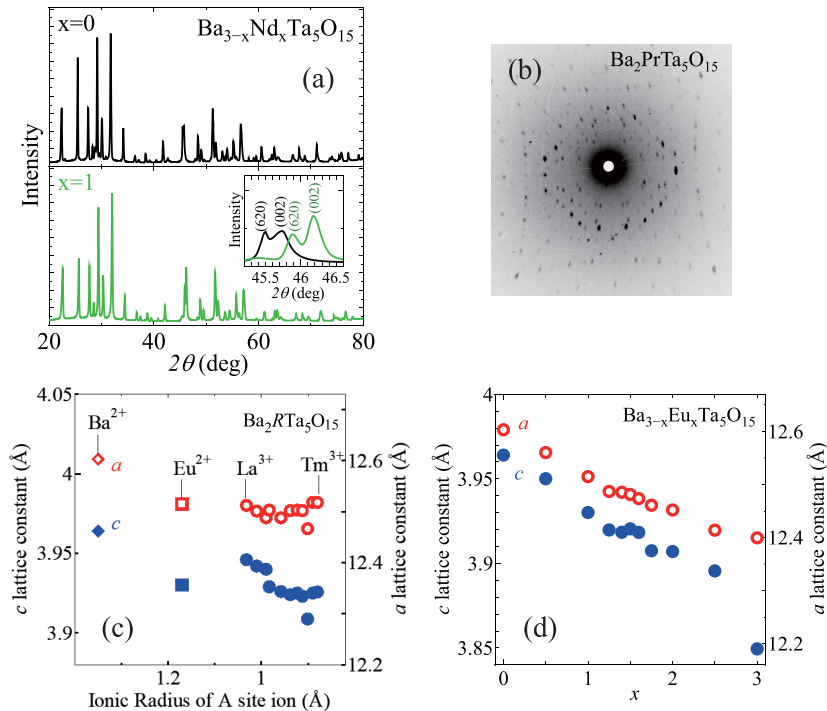
FIG. 4. (a) X-ray diffraction patterns of $Ba_3Ta_5O_{15}$ and $Ba_2NdTa_5O_{15}$. The inset shows an expanded figure for the (620) and (002) peaks. (b) Laue image of $Ba_2PrTa_5O_{15}$ on the ab plane. (c) Lattice constants of $Ba_2RTa_5O_{15}$ as a function of the ionic radius of R. (d) Lattice constants of $Ba_{3-x}Eu_xTa_5O_{15}$ as a function of x.

for $\sigma_a(\omega)$ for both compounds. Such anisotropy in the Drude weight is consistent with the anisotropy observed in resistivity, $\rho_c < \rho_a$. Furthermore, the Drude weight of $Ba_3Ta_5O_{15}$ is approximately by half smaller than that of $Ba_3Nb_5O_{15}$ both for $\sigma_c(\omega)$ and $\sigma_a(\omega)$. The Drude weight is proportional to n/m^*, where n and m^* are the number per unit volume and the effective mass of the conduction carriers, respectively. If n is assumed as the same between the two compounds, the experimental result indicates that the effective mass of the conduction electrons of $Ba_3Ta_5O_{15}$ is approximately two times larger than that of $Ba_3Nb_5O_{15}$.

The magnetic susceptibility of the two compounds with the magnetic field along the c (χ_c) and a (χ_a) axes is shown in Fig. 2(b). Note that the Larmor diamagnetism arising from the core electrons of each atom [46] is subtracted from the data. As can be seen, both χ_c and χ_a of $Ba_3Ta_5O_{15}$ are less than 5×10^{-4} cm^3/mol and almost T independent above 100 K, meaning the Pauli paramagnetism similarly to $Ba_3Nb_5O_{15}$ [8]. The anisotropy of $\chi_c > \chi_a$ for $Ba_3Ta_5O_{15}$ is also the same as that for $Ba_3Nb_5O_{15}$. The Curie tail observed in the $\chi_c(T)$ and $\chi_a(T)$ of $Ba_3Ta_5O_{15}$ amounts to only 0.01 spins per Ta and can be attributed to the defect existing in the crystal.

Next, the data for the compounds with a substitution of various rare earths, $Ba_{3-x}R_xTa_5O_{15}$, are shown. Figure 4(a) shows the x-ray powder diffraction patterns of $Ba_{3-x}Nd_xTa_5O_{15}$ with $x = 0$ and 1. As can be seen, both compounds exhibit similar diffraction patterns. However, the peaks for $x = 1$ shift to higher angles than those for $x = 0$, as more clearly seen in the inset, where the (620) and (002) peaks for both compounds are plotted in an expanded scale. This means decreases in the lattice constants with Nd

substitution, which can be attributed to the smaller ionic radius of Nd than of Ba. A Laue image for a single crystal of $Ba_2PrTa_5O_{15}$ is shown in Fig. 4(b). The lattice constants of $Ba_2RTa_5O_{15}$ with various rare earths R are plotted as a function of the ionic radius of R in Fig. 4(c). The c lattice constants tend to decrease with decreasing ionic radius of R. The lattice constants of $Ba_{3-x}Eu_xTa_5O_{15}$ are plotted as a function of x in Fig. 4(d). Both a and c lattice constants monotonically decrease with increasing x in this series of compounds.

The Ta valence of $Ba_{3-x}R_xTa_5O_{15}$ obtained by TGA is presented in Table I. The nominal Ta valence is $(4.8 - x/5)$ for stoichiometric $Ba_{3-x}R_xTa_5O_{15}$ with trivalent R. As can be seen, the Ta valence obtained by TGA for $Ba_3Ta_5O_{15}$ is 4.77, which is almost consistent with the nominal Ta valence for the parent compound 4.8. However, the Ta valence obtained by TGA increases with increasing x, meaning that the number of $5d$ electrons per Ta rather decreases with R substitution, contrary to expectations based on stoichiometry. Such an increase in the Ta valence (a decrease in the number of $5d$ electrons) indicates an increase in the number of deficient cations Ba and trivalent R with the substitution. Namely, if the exact composition is $Ba_{3-\alpha-x}R_xTa_{5-\beta}O_{15}$, the valence of Ta becomes $(24 - x + 2\alpha)/(5 - \beta)$, which can be larger than 4.8 even with $x > 0$. On the other hand, with the substitution by Eu, which becomes divalent in the present series of compounds as discussed below, the nominal Ta valence should remain 4.8, but as shown in Table I, the Ta valence of $Ba_{3-x}Eu_xTa_5O_{15}$ obtained by TGA also increases with Eu substitution, meaning that the number of $5d$ electrons per Ta decreases.

TABLE I. Ta valence obtained by TGA.

Sample	Nominal valence	Valence by TGA	Number of d electrons per Ta
$Ba_3Ta_5O_{15}$	4.8+	4.74+	0.26
$Ba_2LaTa_5O_{15}$	4.6+	4.85+	0.15
$Ba_2CeTa_5O_{15}$	4.6+	4.88+	0.12
$Ba_2PrTa_5O_{15}$	4.6+	4.86+	0.14
$Ba_2NdTa_5O_{15}$	4.6+	4.88+	0.12
$Ba_2SmTa_5O_{15}$	4.6+	4.86+	0.14
$Ba_2GdTa_5O_{15}$	4.6+	4.85+	0.15
$Ba_2TbTa_5O_{15}$	4.6+	4.89+	0.11
$Ba_2HoTa_5O_{15}$	4.6+	4.89+	0.11
$Ba_2EuTa_5O_{15}$	4.8+	4.90+	0.10
$Ba_{1.75}Eu_{1.25}Ta_5O_{15}$	4.8+	4.83+	0.17
$Ba_{1.5}Eu_{1.5}Ta_5O_{15}$	4.8+	4.87+	0.13
$Ba_{1.4}Eu_{1.6}Ta_5O_{15}$	4.8+	4.87+	0.13

The magnetic susceptibility with the magnetic field (H) along the c axis (χ_c) for $Ba_2RTa_5O_{15}$ on a logarithm scale as a function of T is shown in Fig. 5(a). The magnitude of χ_c at room temperature varies depending on the species of R and is roughly Eu $\sim$ Gd $\sim$ Tb $\sim$ Dy $\sim$ Ho $\sim$ Er $\sim$ Tm $>$ Pr $\sim$ Nd $>$ Ce $>$ Sm. The inverse of the magnetic susceptibility along the c axis and the a axis (χ_a) for R = Ce, Nd, and Eu is shown in Figs. 5(b)–5(d). For these compounds, $1/\chi_c$ and $1/\chi_a$ almost follow the Curie-Weiss behavior $\chi = C/(T + \theta)$. The result of Eu indicates that Eu is divalent with $S = \frac{7}{2}$ but not trivalent, which is nearly nonmagnetic. The behavior of $1/\chi_c$ and $1/\chi_a$ for $Ba_2RTa_5O_{15}$ with other R

elements is summarized also in the Appendix. The Curie constant C obtained by fitting $\chi(T)$ to $\chi = C/(T + \theta)$ is almost consistent with the theoretical values of the magnetic moment for any R, as summarized in Table II in the Appendix. Nevertheless, there is a clear difference in terms of the linearity in $1/\chi(T)$ for each R. Namely, the $1/\chi$ of $Ba_2RTa_5O_{15}$ with R = Eu is quite precisely T linear with almost no anisotropy between χ_c and χ_a, whereas $1/\chi(T)$ for Ce and Nd slightly deviates from a straight line. Such deviation from the Curie-Weiss behavior arises from the contribution of multiplets with higher energies of $4f$ levels, which is negligible for Eu^{2+} in the $4f^7$ configuration. Note that a similar behavior of $1/\chi(T)$ has been observed for $Ba_2RNb_5O_{15}$ [11].

The temperature-dependent resistivity along the c (ρ_c) and a (ρ_a) axes for $Ba_2RTa_5O_{15}$ is shown in Figs. 6(a) and 6(b), respectively. Compared with the parent compound $Ba_3Ta_5O_{15}$, both ρ_c and ρ_a of the R-doped compounds become larger over the entire T range. However, systematic changes in ρ_c and ρ_a with R substitution are barely observed. The absolute values of both ρ_c and ρ_a change quite randomly with R substitution, and the anisotropy of resistivity is also quite random; namely, some compounds show $\rho_c < \rho_a$, which is the case for the
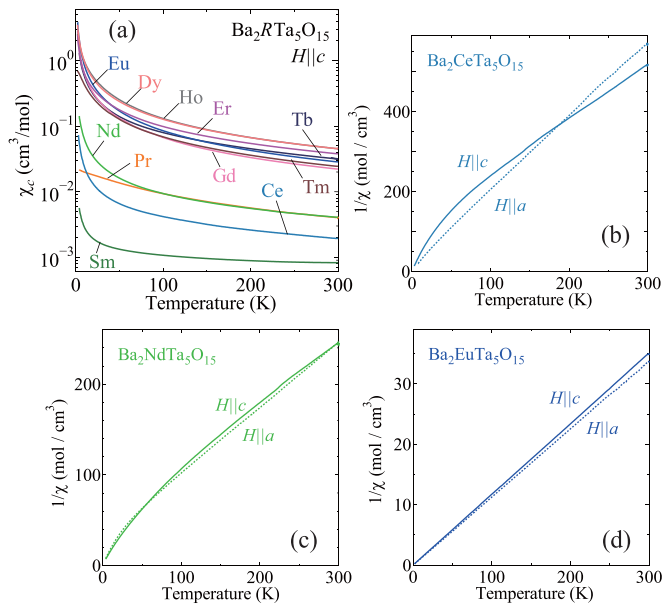

FIG. 5. (a) Temperature dependence of magnetic susceptibility along the c axis on a logarithm scale for $Ba_2RTa_5O_{15}$ with various rare earths. (b)–(d) Temperature dependence of inverse magnetic susceptibility along the c and a axes for $Ba_2RTa_5O_{15}$ with R = (b) Ce, (c) Nd, and (d) Eu.
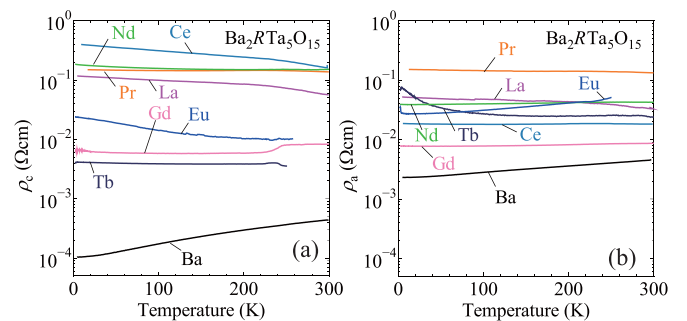

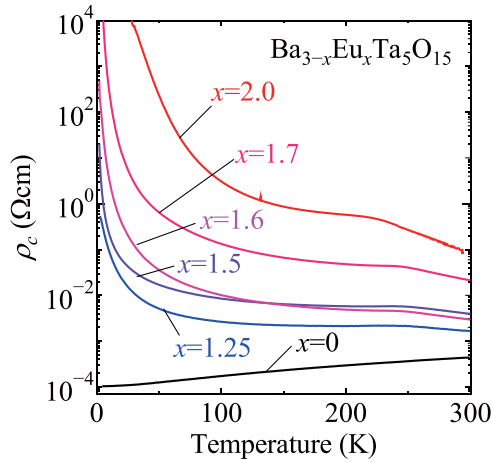FIG. 6. (a), (b) Temperature dependence of resistivity along the (a) c and (b) a axes on a logarithm scale for $Ba_3Ta_5O_{15}$ and $Ba_2RTa_5O_{15}$.

FIG. 7. Temperature dependence of the resistivity along the c axis on a logarithm scale for $Ba_{3-x}Eu_xTa_5O_{15}$ at various x values.

parent compound, whereas other compounds show $\rho_c > \rho_a$. As discussed below, the optical spectra of $Ba_{3-x}R_xTa_5O_{15}$ exhibit a systematic change with R substitution and the same anisotropy as the parent compound. We speculate that the resistivity of $Ba_2RTa_5O_{15}$ is substantially affected by the extrinsic properties of the crystal, for example, the number of defects and, accordingly, it is difficult to discuss its R dependence.

ρ_c at various x values for $Ba_{3-x}Eu_xTa_5O_{15}$ is shown in Fig. 7. In this Eu series, a systematic change in ρ_c with x is observed; namely, ρ_c increases as x increases and ρ_c diverges at the lowest T for the compounds with $x \geqslant 1.7$, meaning that there is a metal-insulator transition at $x_c \sim 1.7$. Note that the Ta valence estimated by TGA increases with Eu substitution, as shown in Table I, but it is still less than 5+, at which it becomes a $5d^0$ band insulator; thus, this metal-insulator transition is not simply caused by a decrease in the nominal number of $5d$ electrons in Ta.

To investigate the carrier density of these compounds, Hall measurement was conducted. Figure 8(a) shows the Hall coefficient along the ac plane R_{ac}, where $j \parallel c$, $E \parallel a$, and $H \parallel b$, and along the ab plane R_{ab}, where $j \parallel a$, $E \parallel b$, and $H \parallel c$, for $Ba_3Ta_5O_{15}$. As can be seen, R_{ac} is negative over the entire T range, indicating that the carriers are electrons. The number of carriers estimated from the absolute value of $R_{ac} \sim 4 \times 10^{-9}$ m^3/C corresponds to $N \sim 0.1$, where N is the number of electrons per Ta, approximately consistent with the number of carriers estimated from the valence of Ta, $N \sim 0.2$. In contrast, R_{ab} is close to zero. Note that a similar anisotropy between R_{ac} and R_{ab} has been observed in $Ba_3Nb_5O_{15}$ [8].

The absolute value of R_{ac} for $Ba_2RTa_5O_{15}$ with $R = $ La and Ce and those for $Ba_{3-x}Eu_xTa_5O_{15}$ with various x values of are presented in Figs. 8(b) and 8(c), respectively. The sign of R_{ac} is negative for all the data. As can be seen, $|R_{ac}|$ increases by several times with La or Ce substitution, and the number of conduction electrons per Ta (N) estimated from R_{ac} by the relation $|R_{ac}| = 1/ne$, where n is the carrier density, becomes ~ 0.02. Such a decrease in the number of conduction electrons with R^{3+} substitution is qualitatively consistent with the
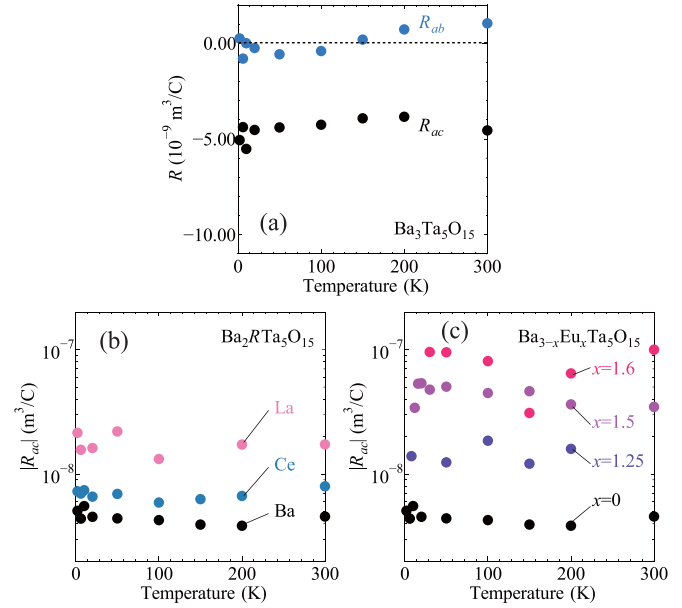

FIG. 8. (a) Hall coefficient as a function of T for $Ba_3Ta_5O_{15}$ along the ac and ab planes. (b), (c) Absolute value of the Hall coefficient along the ac plane for (b) $Ba_2RTa_5O_{15}$ with $R = $ La and Ce and (c) $Ba_{3-x}Eu_xTa_5O_{15}$ with various x values.

increase in the Ta valence estimated by TGA (Table I) caused by off-stoichiometry, although the number of conduction electrons estimated from R_{ac} is smaller than that estimated by TGA, ~ 0.1. For $Ba_{3-x}Eu_xTa_5O_{15}$, as x increases, $|R_{ac}|$ increases, meaning that the number of conduction electrons decreases, and N becomes ~ 0.01 for $x = 1.6$. Such a decrease in the number of conduction electrons estimated from R_{ac} seems to be related to the metal-insulator transition in this series of compounds but cannot be explained simply by the change in the Ta valence estimated by TGA (Table I). It is also to be noted that ρ_c shown in Fig. 7 increases more than $|R_{ac}|$ with x, particularly at low T, indicating that the mobility of the conduction electrons given as $\mu = |R_{ac}|/\rho_c$ decreases with increasing x. This means that not only the number of carriers but their mobility also decreases upon the metal-insulator transition.

The reflectivity spectra $R_c(\omega)$ and $R_a(\omega)$ for $Ba_3Ta_5O_{15}$, $Ba_2LaTa_5O_{15}$, and $Ba_{3-x}Eu_xTa_5O_{15}$ with $x = 1$, 1.5, and 1.75 are shown in Figs. 9(a) and 9(b), respectively. With R substitution, both $R_c(\omega)$ and $R_a(\omega)$ below 1 eV decrease, and the plasma edge shifts to lower frequencies. Below the plasma edge, $R_c(\omega)$ is higher than $R_a(\omega)$ even with R substitution. The optical conductivity spectra $\sigma_c(\omega)$ and $\sigma_a(\omega)$ obtained by the Kramers-Kronig transformation of $R_c(\omega)$ and $R_a(\omega)$ are shown in Figs. 9(c) and 9(d), respectively. The R substitution results in decreases in $\sigma_c(\omega)$ and $\sigma_a(\omega)$ below 1 eV. In particular, the spectral weight below 1 eV for $Ba_{3-x}Eu_xTa_5O_{15}$ with $x = 1.5$ and 1.75 is substantially suppressed and becomes less than $\frac{1}{10}$ of that for the parent compound. Nevertheless, the spectral weight of such a Drude component for $\sigma_c(\omega)$ is larger than that for $\sigma_a(\omega)$ for all the compounds. The reflectivity and optical conductivity spectra of $Ba_2RTa_5O_{15}$ with other R elements are summarized in the Appendix, and the behavior is similar to that of $Ba_2LaTa_5O_{15}$; namely, $\sigma_c(\omega)$ and $\sigma_a(\omega)$
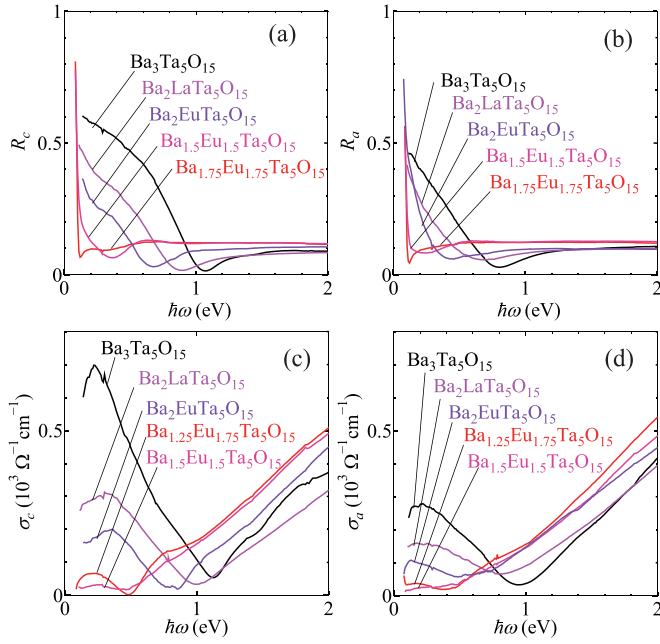
FIG. 9. (a), (b) Reflectivity spectra with the polarization along the (a) c and (b) a axes, and (c), (d) optical conductivity spectra along the (c) c and (d) a axes for $Ba_3Ta_5O_{15}$, $Ba_2LaTa_5O_{15}$, and $Ba_{3-x}Eu_xTa_5O_{15}$ with $x = 1$, 1.5, and 1.75.

below 1 eV decrease with R substitution, but $\sigma_c(\omega)$ remains larger than $\sigma_a(\omega)$. This means that the anisotropy of optical conductivity does not change with any R substitution, unlike the anisotropy of the dc resistivity shown in Fig. 6.

The Drude weight for $\sigma_c(\omega)$ and the number of electrons per Ta (N) estimated from the Hall coefficient at 100 K are plotted on a logarithm scale as functions of x for $Ba_{3-x}Eu_xTa_5O_{15}$ in Figs. 10(a) and 10(b), respectively, together with the results for the Nb series $Ba_{3-x}Eu_xNb_5O_{15}$ [11]. As can be seen, both values decrease by more than one order of magnitude between $x = 0$ and 1.6 for $Ba_{3-x}Eu_xTa_5O_{15}$. This indicates that the x dependence of the Drude weight, which is proportional to n/m^*, in this series
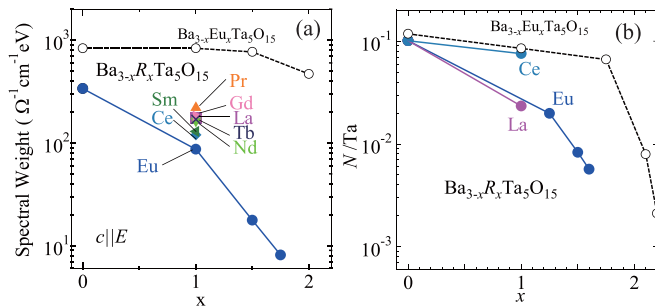

FIG. 10. (a) Drude weight [the integral of $\sigma(\omega)$ up to the first minimum position], and (b) the number of electrons per Ta (N) estimated from the Hall coefficient, both on a logarithm scale as functions of x for $Ba_{3-x}Eu_xTa_5O_{15}$ (closed symbols and solid lines) and for $Ba_{3-x}Eu_xNb_5O_{15}$ (open circles and dashed lines). N is estimated by the Hall coefficient at 100 K for the Ta series and that at 30 K for the Nb series.
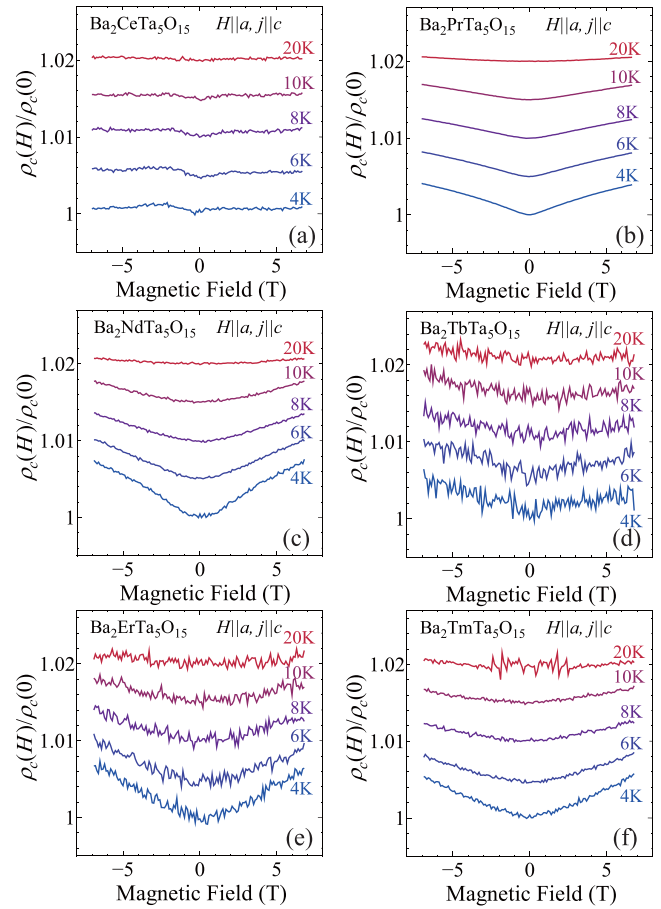

FIG. 11. Resistivity along the c axis normalized to the value at $H = 0$, $\rho_c(H)/\rho_c(0)$, as a function of the magnetic field $H \parallel a$ for $Ba_2RTa_5O_{15}$ with $R =$ Ce, Pr, Nd, Tb, Er, and Tm.

of compounds is principally dominated by the decrease in the number of electrons. It is also found that both the Drude weight and the number of electrons estimated from the Hall coefficient decrease much more slowly with x for the Nb series.

Figure 11 shows the dependence of resistivity along the c axis normalized to the value at $H = 0$ on the magnetic field along the a axis for $Ba_2RTa_5O_{15}$ with trivalent R. The compounds with any of trivalent R exhibit a small positive magnetoresistance, which increases with decreasing T but is less than 1% at 4 K with an applied magnetic field of 7 T. Figure 12(a) shows the H dependence of ρ_c normalized to the value at $H = 0$ for $Ba_{3-x}Eu_xTa_5O_{15}$ with $x = 1.6$. This compound exhibits a large negative magnetoresistance, whose magnitude defined as $1 - \rho_c(H)/\rho_c(0)$ increases with decreasing temperature and is ~ 0.8 at 4 K.

The H dependence of ρ_c normalized to the value at $H = 0$ for $Ba_{3-x}Eu_xTa_5O_{15}$ with various x values at 4 K is shown in Fig. 12(b). The magnitude of negative magnetoresistances, $1 - \rho_c(H)/\rho_c(0)$, is only ~ 0.02 for $x = 1.0$, but it gradually increases with x and becomes ~ 0.9 for $x = 1.7$. In Fig. 12(c), $\rho_c(0)/\rho_c(7$ T$)$ is plotted as a function of x at various T values. As can be seen, $\rho_c(0)/\rho_c(7$ T$)$ at low T is enhanced
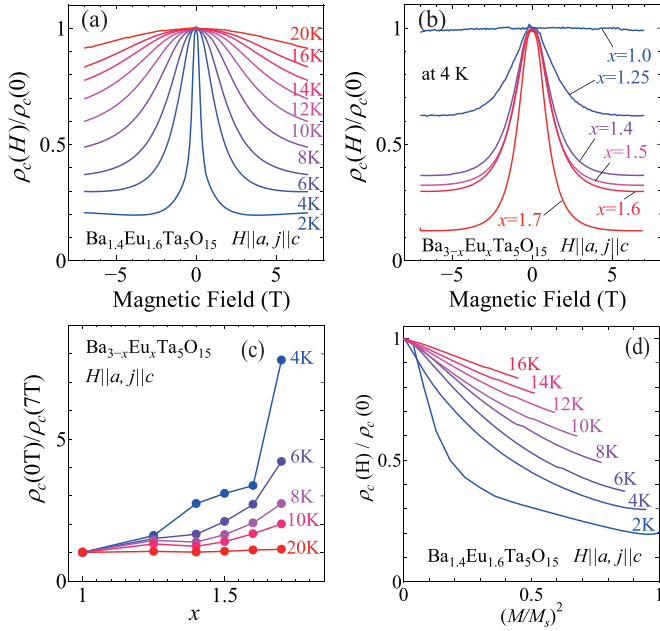
FIG. 12. (a), (b) Resistivity along the c axis normalized to the value at $H = 0$, $\rho_c(H)/\rho_c(0)$, as a function of the magnetic field $H \parallel a$ for $Ba_{3-x}Eu_xTa_5O_{15}$ (a) with $x = 1.6$ at various T values and (b) at 4 K with various x values. (c) Dependence of $\rho_c(0)/\rho_c(7\ T)$ on x at various T values for $Ba_{3-x}Eu_xTa_5O_{15}$. (d) $\rho_c(H)/\rho_c(0)$ as a function of the magnetization M for $Ba_{3-x}Eu_xTa_5O_{15}$ with $x = 1.6$.

FIG. 13. Energy diagrams of (a) $Ba_3Ta_5O_{15}$, (b) $Ba_3Nb_5O_{15}$, (c) $Ba_2RTa_5O_{15}$, (d) $Ba_{3-x}Eu_xTa_5O_{15}$, and (e) $Ba_{3-x}Eu_xNb_5O_{15}$.

near the metal-insulator phase boundary of $x_c = 1.7$, where $\rho_c(0)/\rho_c(7\ T)$ reaches the maximum of ~ 8.

For the Nb series, $Ba_{3-x}Eu_xNb_5O_{15}$, if $\rho_c(H)/\rho_c(0)$ values at various T values are plotted as a function of the magnetization M, they almost merge at $x = 2.0$ [9], where the magnitude of negative magnetoresistance, $\rho_c(0)/\rho_c(H)$, at 7 T and 4 K is ~ 5, but they do not merge at $x = 2.2$ [11], where $\rho_c(0)/\rho_c(H)$ at 7 T and 4 K is ~ 500, probably because an insulator-metal transition is induced by a magnetic field near the metal-insulator phase boundary. In Fig. 12(d), $\rho_c(H)/\rho_c(0)$ at various T values is plotted as a function of the magnetization M for $Ba_{3-x}Eu_xTa_5O_{15}$ with $x = 1.6$. As can be seen, the data at different values of T do not merge, although $\rho_c(0)/\rho_H(0)$ at 7 T and 4 K is only ~ 4. This indicates that even if the system is sufficiently close to the metal-insulator phase boundary to induce the magnetic-field-induced insulator-metal transition, the magnitude of negative magnetoresistance is smaller for the Ta series than for the Nb series.

IV. DISCUSSION

We compare the properties of $Ba_{3-x}R_xTa_5O_{15}$ and $Ba_{3-x}R_xNb_5O_{15}$ [11]. First, the Drude weight of $Ba_3Ta_5O_{15}$ is approximately half that of $Ba_3Nb_5O_{15}$, meaning that the effective mass of the conduction electrons in $Ba_3Ta_5O_{15}$ is two times larger than that of $Ba_3Nb_5O_{15}$. This cannot be explained by the larger extent in the space of Ta $5d$ orbitals than of Nb $4d$ orbitals, which results in a larger transfer integral. However, as illustrated in Figs. 13(a) and 13(b), it is likely that the Ta $5d$ orbitals are located higher in energy than the Nb $4d$
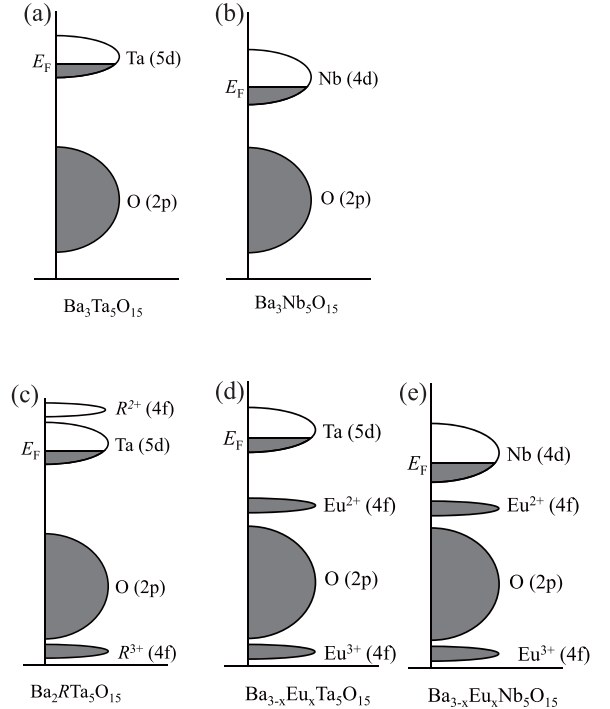
orbitals (by ~ 0.5 eV according to Ref. [47]); thus, the energy difference between the cation d orbitals and the oxygen $2p$ orbitals is larger for $Ba_3Ta_5O_{15}$ than for $Ba_3Nb_5O_{15}$, resulting in a smaller hybridization between the two orbitals and the dispersion of the conduction band mainly composed of Ta $5d$ levels, which is consistent with the experimental result.

The substitution of Ba by trivalent rare earths R causes different situations between the Ta and Nb series. For $Ba_3Nb_5O_{15}$, the R substitution induces an increase in the number of conduction electrons per Nb, as expected, and this is confirmed by the decrease in the absolute Hall coefficient value [11]. For $Ba_3Ta_5O_{15}$, however, the R substitution induces a decrease in the number of conduction electrons per Ta (Table I), probably due to the increase in the number of cation deficiencies. Such a decrease in the number of conduction electrons is consistent with the increase in the absolute Hall coefficient values and the decrease in the Drude weight experimentally observed (Figs. 8–10).

The substitution of Ba by divalent Eu results in a metal-insulator transition both for the Ta and Nb series. The metal-insulator phase boundary x_c is ~ 1.7 for the Ta series, whereas it is ~ 2.2 for the Nb series [11]. For the metal-insulator transition in the Nb series, it is proposed that when R occupies a site that is loosely bound to surrounding oxygen ions, several energy minima appear at which R can settle, resulting in disorder and the insulating state [8,11]. Based on this consideration, the origin of the difference in x_c between the Ta and Nb series can be qualitatively explained by the fact that for the Ta series, the band dispersion of the parent compound is smaller, meaning that the itinerancy of the conduction electrons is smaller, resulting in the predominance of the insulating phase and a smaller x_c. Another difference between the
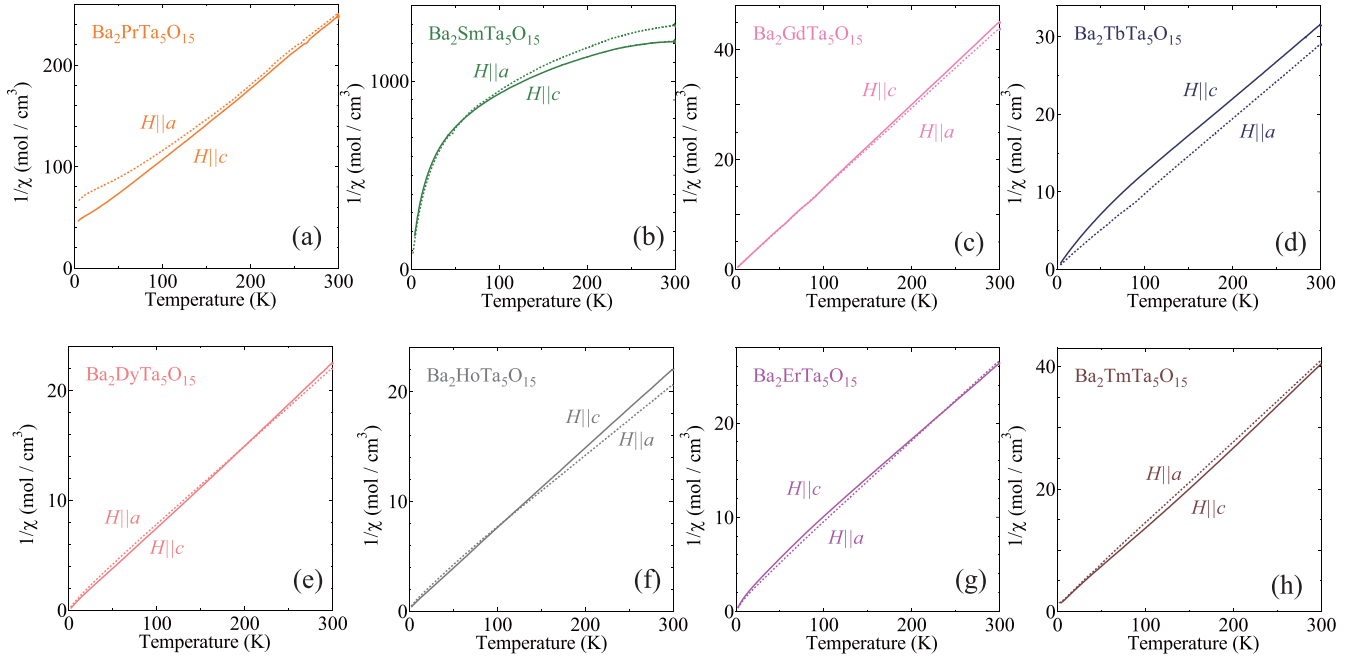
FIG. 14. Inverse magnetic susceptibility along the c (solid lines) and a (dashed lines) axes for $Ba_2RNb_5O_{15}$ with $R =$ Pr, Sm, Gd, Tb, Dy, Ho, Er, and Tm.

two series of compounds is seen in the x dependence of the Drude weight, which decreases much more substantially with x for the Ta series [Fig. 10(a)].

Regarding the negative magnetoresistance, both for the Ta and Nb series, its absolute value increases at low T and near x_c. The largest negative magnetoresistance, $\rho(0)/\rho(H)$, is $\sim 10^4$ for the Nb series, whereas it is ~ 8 for the Ta series. This suggests that the coupling between the d electrons in the transition metal and the localized spins in Eu is smaller for the Ta series. As discussed above, the Ta 5d orbitals are located higher in energy than the Nb 4d orbitals [47] and, thus, the energy difference between the Eu^{2+} level and the Ta 5d orbitals is larger than that between the Eu^{2+} level and the Nb 4d orbitals, as illustrated in Figs. 13(d) and 13(e). This results in a smaller exchange coupling between the Eu spins and the electrons in the Ta 5d levels, which is dominated by $t_{df}^2/(E_d - E_f)$, where E_d, E_f, and t_{df} are the energy of the d states of Ta/Nb, the energy of Eu^{2+} levels, and the transfer integral between these two states, respectively. This may also result in the difference in the T dependence of the Hall coefficient R_{ac} between the Nb series, where $|R_{ac}|$ increases with a decrease in T [11], and the Ta series, where it is almost T independent even near x_c, as shown in Fig. 8(c). It is to be noted that the discussion above is based on the ionic model but ignores the effect of the 2p states of the ligand oxygens, which may play an important role for the different behavior between the Ta and Nb series. Furthermore, the effect of magnetic polarons, which appear if a small number of carriers exist in a large number of spins, may play a role in the Ta series, as seen in various Eu chalcogenides [17–20] and $Ba_{3-x}Eu_xNb_5O_{15}$ [11].

Regarding the R dependence of magnetoresistance in $Ba_{3-x}R_xTa_5O_{15}$, only the compounds with Eu substitution

exhibit a large negative magnetoresistance, whereas those with a substitution by other trivalent R exhibit only a small positive magnetoresistance. According to a recent photoemission spectroscopy of $Ba_{3-x}Eu_xNb_5O_{15}$, the Eu^{2+} level is located at ~ 2 eV below the Fermi level (E_F) [12], and it is likely that for $Ba_{3-x}Eu_xTa_5O_{15}$, the Eu^{2+} level is located slightly lower in energy than this. Thus, we can draw the energy diagram shown in in Figs. 13(c) and 13(d), and we speculate that the energy difference between E_F and the R^{3+} level is much larger than that between E_F and the Eu^{2+} level, resulting in a much smaller exchange coupling between the localized moments of the 4f electrons in R^{3+} and the 5d electrons in Ta.

V. SUMMARY

Single crystals of tantalates with a tetragonal tungsten bronze structure $Ba_3Ta_5O_{15}$ and with a substitution of Ba by trivalent rare earth R ($Ba_2RTa_5O_{15}$) and divalent Eu ($Ba_{3-x}Eu_xTa_5O_{15}$) have been grown and studied. It was found that $Ba_3Ta_5O_{15}$ is metallic due to the 0.2 electrons in the Ta 5d orbitals, and its resistivity is lower along the c axis, similarly to its Nb analog, $Ba_3Nb_5O_{15}$. The Drude weight of the optical conductivity spectrum for $Ba_3Ta_5O_{15}$ is approximately half that for $Ba_3Nb_5O_{15}$, indicating that the effective mass of the conduction carriers is two times heavier.

With a substitution of Ba by trivalent R, the Ta valence increases, meaning that the number of 5d electrons decreases, contrary to the expectation based on the stoichiometry of the compounds. This is likely caused by the increases in the number of deficient cations (Ba and Ta) with R substitution. The Drude weight also decreases, but the Drude weight along the c axis remains larger than that along the a axis with R substitution. However, the resistivity of $Ba_2RTa_5O_{15}$ does not
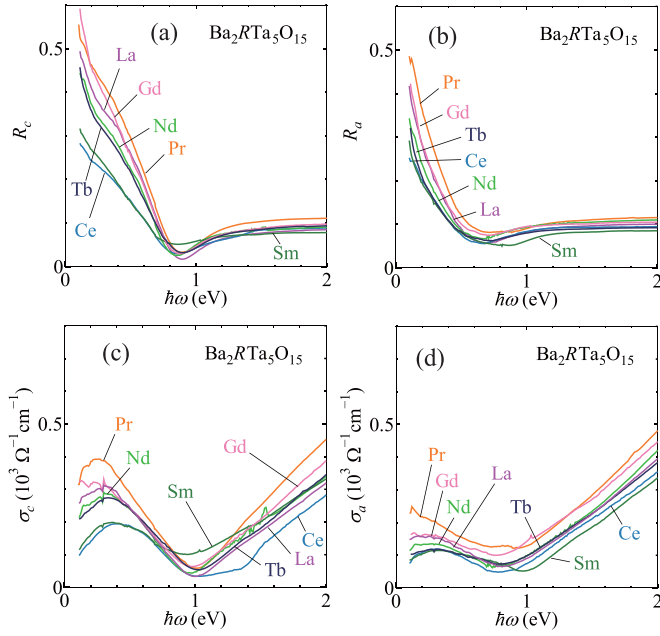
FIG. 15. (a), (b) Reflectivity spectra with the polarization along the (a) c and (b) a axes, and (c), (d) optical conductivity spectra along the (c) c and (d) a axes for $Ba_2RNb_5O_{15}$ with $R = La$, Ce, Pr, Nd, Sm, Gd, and Tb.

systematically change with R substitution, suggesting that the dc resistivity of this series of compounds is dominated by extrinsic properties, for example, disorders in the crystals.

On the other hand, the resistivity of $Ba_{3-x}Eu_xTa_5O_{15}$ systematically increases with increasing x, and it exhibits a metal-insulator transition at $x_c \sim 1.7$. This behavior is also similar to its Nb analog, $Ba_{3-x}Eu_xNb_5O_{15}$, although the critical value of x for the metal-insulator transition is larger for the Eu series, $x_c \sim 2.2$, probably due to the larger itinerancy of the d electrons in $Ba_3Nb_5O_{15}$. The absolute values of the Hall coefficient for $Ba_{3-x}Eu_xTa_5O_{15}$ increase near the metal-insulator phase boundary, indicating that this metal-insulator transition is caused by the decrease in the number of the conduction carriers. Unlike the case of the Nb series, however, the increase in the absolute values of the Hall coefficient with decreasing T is barely observed in the Ta series. The Drude weight of $Ba_{3-x}Eu_xTa_5O_{15}$ also decreases near the metal-insulator phase boundary.

Regarding magnetoresistance of $Ba_{3-x}R_xTa_5O_{15}$ with various R, only the compounds with divalent Eu exhibit a large negative magnetoresistance, whereas those with trivalent R exhibit only a small positive magnetoresistance. The magnitude of negative magnetoresistance of $Ba_{3-x}Eu_xTa_5O_{15}$ increases to $\rho(0)/\rho(H) \sim 8$ near the metal-insulator phase boundary, which is smaller than that of the Nb series. This

difference between the Ta and Nb series can be explained by

TABLE II. Effective moment of R, p, and the Weiss temperature θ obtained by the fitting of the magnetic susceptibility of $Ba_2RNb_5O_{15}$ to $\chi = C/(T + \theta)$.

R	p	θ (K)	Theoretical p
Ce^{3+}	2.32	76.6	2.54
Pr^{3+}	3.45	59.5	3.58
Nd^{3+}	3.52	79.8	3.62
Sm^{3+}	3.14	1300	0.84
Eu^{2+}	8.27	0.2	7.94
Gd^{3+}	7.30	0.2	7.94
Tb^{3+}	9.18	32.2	9.72
Dy^{3+}	10.28	−2.2	10.63
Ho^{3+}	10.1	8.2	10.60
Er^{3+}	9.92	25.7	9.59
Tm^{3+}	7.25	8.3	7.54

the fact that the Ta $5d$ orbitals are located higher in energy than the Nb $4d$ orbitals. This results in (1) a larger energy difference between the cation d orbitals and the oxygen $2p$ orbitals, resulting in a smaller hybridization and a smaller bandwidth of the conduction band, and (2) a larger energy difference between the cation d orbitals and the Eu^{2+} $4f$ level, resulting in a smaller magnetic coupling between the Ta conduction electrons and the Eu localized spins. The absence of negative magnetoresistance in the compounds with trivalent R can be explained by the fact that the R^{3+} $4f$ level is located in a much deeper position in energy than the Eu^{2+} $4f$ level, resulting in a negligible interaction between the Ta conduction electrons and the R^{3+} localized spins.

APPENDIX

Inverse magnetic susceptibility as a function of T for $Ba_2RNb_5O_{15}$ with various R both along the c and a axes is shown in Fig. 14. The reflectivity and optical conductivity spectra of $Ba_2RNb_5O_{15}$ with $R = La$, Ce, Pr, Nd, Sm, Gd, and Tb are shown in Fig. 15. The effective moment of R (p) obtained from the magnetic susceptibility of $Ba_2RNb_5O_{15}$ is shown in Table II.

[1] B. Hessen, S. A. Sunshine, T. Siegrist, A. T. Fiory, and J. V. Waszczak, Structure and properties of reduced barium niobium oxide single crystals obtained from borate fluxes, Chem. Mater. **3**, 528 (1991).

[2] Y. K. Hwang and Y.-U. Kwon, Syntheses and electrical properties of tetragonal tungsten bronze type solid solution $Ba_{6-x}La_xNb_{10}O_{30+\delta}$ ($x = 0, 1, 2, 3$) and $Sr_6Nb_{10}O_{30}$, Mater. Res. Bull. **32**, 1495 (1997).

[3] E. Castel, P. Veber, M. Albino, M. Velázquez, S. Pechev, D. Denux, J. Chaminade, M. Maglione, and M. Josse, Crystal growth and characterization of tetragonal tungsten bronze ferroniobates $Ba_2LnFeNb_4O_{15}$, J. Cryst. Growth **340**, 156 (2012).

[4] H. Ma, K. Lin, L. Liu, B. Yang, Y. Rong, J. Chen, J. Deng, S. Kawaguchi, K. Kato, and X. Xing, Structure and electrical properties of tetragonal tungsten bronze $Ba_2CeFeNb_4O_{15}$, RSC Adv. **5**, 76957 (2015).

[5] T. Kolodiazhnyi, H. Sakurai, O. Vasylkiv, H. Borodianska, and Y. Mozharivskyj, Abnormal thermal conductivity in tetragonal tungsten bronze $Ba_{6-x}Sr_xNb_{10}O_{30}$, Appl. Phys. Lett. **104**, 111903 (2014).

[6] T. Kolodiazhnyi, H. Sakurai, M. Isobe, Y. Matsushita, S. Forbes, Y. Mozharivskyj, T. J. S. Munsie, G. M. Luke, M. Gurak, and D. R. Clarke, Superconductivity and crystal structural origins of the metal-insulator transition in $Ba_{6-x}Sr_xNb_{10}O_{30}$ tetragonal tungsten bronzes, Phys. Rev. B **92**, 214508 (2015).

[7] T. Yasuda, Y. Kondo, T. Kajita, K. Murota, D. Ootsuki, Y. Takagi, A. Yasui, N. L. Saini, T. Katsufuji, and T. Mizokawa, Interplay between electronic correlation and atomic disorder in a low carrier density $4d$ transition-metal oxide, Phys. Rev. B **102**, 205133 (2020).

[8] Y. Kondoh, R. Takei, T. Okuda, K. Ueno, Y. Katayama, T. Saiki, W. Sekino, T. Kajita, and T. Katsufuji, Metal-insulator transition in $Ba_{3-x}Sr_xNb_5O_{15}$, Phys. Rev. B **104**, 125128 (2021).

[9] K. Iwamoto, W. Sekino, S. Ito, Y. Katayama, K. Ueno, and T. Katsufuji, Large negative magnetoresistance in $Ba_{3-x}Eu_xNb_5O_{15}$, J. Phys. Soc. Jpn. **91**, 033702 (2022).

[10] R. Nakamura, T. Miyoshino, Y. Kondoh, T. Kajita, T. Katsufuji, N. L. Saini, and T. Mizokawa, Electronic structure of $Ba_3Nb_5O_{15}$ and $Ba_2SrNb_5O_{15}$ studied by band calculation and photoemission spectroscopy, J. Phys. Soc. Jpn. **91**, 064711 (2022).

[11] W. Sekino, R. Takei, S. Ito, H. Takei, K. Iwamoto, Y. Katayama, K. Ueno, H. Kuwahara, and T. Katsufuji, Charge transport, specific heat, and optical properties across the metal-insulation transition in $Ba_{3-x}R_xNb_5O_{15}$, Phys. Rev. Mater. **7**, 124404 (2023).

[12] R. Nakamura, D. Takegami, A. Melendez-Sans, L. H. Tjeng, T. Miyoshino, K. Iwamoto, W. Sekino, M. Yoshimura, K.-D. Tsuei, T. Katsufuji, and T. Mizokawa, Interplay between strongly localized Eu $4f$ and weakly localized Nb $4d$ electrons in $Eu_3Nb_5O_{15}$, Phys. Rev. B **109**, 165148 (2024).

[13] S. Nakatsuji and Y. Maeno, Quasi-two-dimensional Mott transition system $Ca_{2-x}Sr_xRuO_4$, Phys. Rev. Lett. **84**, 2666 (2000).

[14] V. I. Anisimov, I. A. Nekrasov, D. E. Kondakov, T. M. Rice, and M. Sigrist, Orbital-selective Mott-insulator transition in $Ca_{2-x}Sr_xRuO_4$, Eur. Phys. J. B **25**, 191 (2002).

[15] N. Ali, M. Hill, S. Labroo, and J. Greedan, Magnetic and electrical properties of $R_2Mo_2O_7$ pyrochlore compounds, J. Solid State Chem. **83**, 178 (1989).

[16] T. Katsufuji, H. Y. Hwang, and S.-W. Cheong, Anomalous magnetotransport properties of $R_2Mo_2O_7$ near the magnetic phase boundary, Phys. Rev. Lett. **84**, 1998 (2000).

[17] T. R. McGuire and M. W. Shafer, Ferromagnetic europium compounds, J. Appl. Phys. **35**, 984 (1964).

[18] S. Von Molnar and S. Methfessel, Giant Negative Magnetoresistance in Ferromagnetic $Eu_{1-x}Gd_xSe$, J. Appl. Phys. **38**, 959 (1967).

[19] M. R. Oliver, J. O. Dimmock, A. L. McWhorter, and T. B. Reed, Conductivity studies in europium oxide, Phys. Rev. B **5**, 1078 (1972).

[20] A. Mauger, M. Escorne, C. Godart, J. P. Desfours, and J. C. Achard, Magnetic properties of gd doped EuO single crystals, J. Phys. Colloq. **41**, C5-263 (1980).

[21] J. S. Moodera, X. Hao, G. A. Gibson, and R. Meservey, Electron-spin polarization in tunnel junctions in zero applied field with ferromagnetic EuS barriers, Phys. Rev. Lett. **61**, 637 (1988).

[22] T. S. Santos and J. S. Moodera, Observation of spin filtering with a ferromagnetic EuO tunnel barrier, Phys. Rev. B **69**, 241203(R) (2004).

[23] T. Katsufuji and Y. Tokura, Transport and magnetic properties of a ferromagnetic metal: $Eu_{1-x}R_xTiO_3$, Phys. Rev. B **60**, R15021 (1999).

[24] Y. Tomioka, T. Ito, and A. Sawa, Magnetotransport properties of $Eu_{1-x}La_xTiO_3$ ($0 \leqslant x \leqslant 0.07$) single crystals, J. Phys. Soc. Jpn. **87**, 094716 (2018).

[25] K. Momma and F. Izumi, *VESTA* 3 for three-dimensional visualization of crystal, volumetric and morphology data, J. Appl. Crystallogr. **44**, 1272 (2011).

[26] C. R. Feger and R. P. Ziebarth, Synthesis and structural characterization of reduced ternary tantalum oxides in the tetragonal tungsten bronze structure, Chem. Mater. **7**, 373 (1995).

[27] T. Siegrist, R. Cava, and J. Krajewski, Reduced alkaline earth tantalates, Mater. Res. Bull. **32**, 881 (1997).

[28] J.-Y. Kim and Y.-I. Kim, Local structure and dielectric behavior of tetragonal tungsten bronzes β-$SrTa_2O_6$ and β'-$SrTa_2O_6$, J. Ceram. Soc. Jpn. **123**, 419 (2015).

[29] Y.-H. Du, W. Zeng, B. Tang, F.-S. Liu, Q.-J. Liu, X.-H. Li, and M. Zhong, Density functional theory study on the structural, electronic, optical and photocatalytic properties of $BaTa_2O_6$, $Ba_2Ta_{15}O_{32}$, $Ba_3Ta_5O_{15}$ and $Ba_5Ta_4O_{15}$, J. Solid State Chem. **298**, 122127 (2021).

[30] C. J. Raub, A. R. Sweedler, M. A. Jensen, S. Broadston, and B. T. Matthias, Superconductivity of sodium tungsten bronzes, Phys. Rev. Lett. **13**, 746 (1964).

[31] K. Ohgushi, A. Yamamoto, Y. Kiuchi, C. Ganguli, K. Matsubayashi, Y. Uwatoko, and H. Takagi, Superconducting phase at 7.7 K in the Hg_xReO_3 compound with a hexagonal bronze structure, Phys. Rev. Lett. **106**, 017001 (2011).

[32] N. Haldolaarachchige, Q. Gibson, J. Krizan, and R. J. Cava, Superconducting properties of the K_xWO_3 tetragonal tungsten bronze and the superconducting phase diagram of the tungsten bronze family, Phys. Rev. B **89**, 104520 (2014).

[33] M. Hanawa, Y. Muraoka, T. Tayama, T. Sakakibara, J. Yamaura, and Z. Hiroi, Superconductivity at 1 K in $Cd_2Re_2O_7$, Phys. Rev. Lett. **87**, 187001 (2001).

[34] J. Harter, Z. Zhao, J.-Q. Yan, D. Mandrus, and D. Hsieh, A parity-breaking electronic nematic phase transition in the spin-orbit coupled metal $Cd_2Re_2O_7$, Science **356**, 295 (2017).

[35] D. Mandrus, J. R. Thompson, R. Gaal, L. Forro, J. C. Bryan, B. C. Chakoumakos, L. M. Woods, B. C. Sales, R. S. Fishman, and V. Keppens, Continuous metal-insulator transition in the pyrochlore $Cd_2Os_2O_7$, Phys. Rev. B **63**, 195104 (2001).

[36] Y. G. Shi, Y. F. Guo, S. Yu, M. Arai, A. A. Belik, A. Sato, K. Yamaura, E. Takayama-Muromachi, H. F. Tian, H. X. Yang, J. Q. Li, T. Varga, J. F. Mitchell, and S. Okamoto, Continuous

metal-insulator transition of the antiferromagnetic perovskite NaOsO$_3$, Phys. Rev. B **80**, 161104(R) (2009).

[37] Z. Hiroi, J.-i. Yamaura, and K. Hattori, Rattling good superconductor: β-pyrochlore oxides AOs$_2$O$_6$, J. Phys. Soc. Jpn. **81**, 011012 (2012).

[38] B. J. Kim, H. Jin, S. J. Moon, J. Y. Kim, B.-G. Park, C. S. Leem, J. Yu, T. W. Noh, C. Kim, S. J. Oh, J. H. Park, V. Durairaj, G. Cao, and E. Rotenberg, Novel $J_{\text{eff}} = 1/2$ Mott state induced by relativistic spin-orbit coupling in Sr$_2$IrO$_4$, Phys. Rev. Lett. **101**, 076402 (2008).

[39] S. J. Moon, H. Jin, K. W. Kim, W. S. Choi, Y. S. Lee, J. Yu, G. Cao, A. Sumi, H. Funakubo, C. Bernhard, and T. W. Noh, Dimensionality-controlled insulator-metal transition and correlated metallic state in 5d transition metal oxides Sr$_{n+1}$Ir$_n$O$_{3n+1}$ ($n = 1, 2$, and ∞), Phys. Rev. Lett. **101**, 226402 (2008).

[40] K. Matsuhira, M. Wakeshima, R. Nakanishi, T. Yamada, A. Nakamura, W. Kawano, S. Takagi, and Y. Hinatsu, Metal-insulator transition in pyrochlore iridates Ln_2Ir$_2$O$_7$ (Ln = Nd, Sm, and Eu), J. Phys. Soc. Jpn. **76**, 043706 (2007).

[41] K. Matsuhira, M. Wakeshima, Y. Hinatsu, and S. Takagi, Metal-insulator transitions in pyrochlore oxides Ln$_2$Ir$_2$O$_7$, J. Phys. Soc. Jpn. **80**, 094701 (2011).

[42] K. Ueda, J. Fujioka, and Y. Tokura, Variation of optical conductivity spectra in the course of bandwidth-controlled metal-insulator transitions in pyrochlore iridates, Phys. Rev. B **93**, 245120 (2016).

[43] K. Kitamura, N. II, I. Shindo, and S. Kimura, Interface shape and horizontal variations of Al and Ga contents in substituted YIG single crystals grown by the floating zone method, J. Cryst. Growth **46**, 277 (1979).

[44] C.-H. Lee, N. Kaneko, S. Hosoya, K. Kurahashi, S. Wakimoto, K. Yamada, and Y. Endoh, Growth of large single crystals using the improved lamp-image floating-zone furnace: Application to La$_{2-x}$Sr$_x$CuO$_4$, Supercond. Sci. Technol. **11**, 891 (1998).

[45] H. Xu, Y. Jiang, X. Fan, Y. Wang, and G. Liu, Growth and dielectric properties of Ta$_2$O$_5$ single crystal by the floating zone method, Cryst. Res. Technol. **47**, 903 (2012).

[46] Q. Chen, Z. Li, B. Miao, X. Zhang, and S. Zhang, Ta$_2$O$_5$ nanocrystals strengthened linear, nonlinear, and Faraday properties of heavy metal oxide diamagnetic material, J. Am. Ceram. Soc. **105**, 225 (2022).

[47] W. A. Harrison, *Electronic Structure and the Properties of Solids: The Physics of the Chemical Bond* (Dover, New York, 1989).